Investigation of the Mechanical Performance of Compliant Thermal Barriers

Jeffrey J. DeMange
The University of Toledo, Toledo, Ohio

Robert J. Bott
Case Western Reserve University, Cleveland, Ohio

Patrick H. Dunlap
Glenn Research Center, Cleveland, Ohio

NASA STI Program . . . in Profile

Since its founding, NASA has been dedicated to the advancement of aeronautics and space science. The NASA Scientific and Technical Information (STI) program plays a key part in helping NASA maintain this important role.

The NASA STI Program operates under the auspices of the Agency Chief Information Officer. It collects, organizes, provides for archiving, and disseminates NASA's STI. The NASA STI program provides access to the NASA Aeronautics and Space Database and its public interface, the NASA Technical Reports Server, thus providing one of the largest collections of aeronautical and space science STI in the world. Results are published in both non-NASA channels and by NASA in the NASA STI Report Series, which includes the following report types:

- TECHNICAL PUBLICATION. Reports of completed research or a major significant phase of research that present the results of NASA programs and include extensive data or theoretical analysis. Includes compilations of significant scientific and technical data and information deemed to be of continuing reference value. NASA counterpart of peer-reviewed formal professional papers but has less stringent limitations on manuscript length and extent of graphic presentations.

- TECHNICAL MEMORANDUM. Scientific and technical findings that are preliminary or of specialized interest, e.g., quick release reports, working papers, and bibliographies that contain minimal annotation. Does not contain extensive analysis.

- CONTRACTOR REPORT. Scientific and technical findings by NASA-sponsored contractors and grantees.

- CONFERENCE PUBLICATION. Collected papers from scientific and technical conferences, symposia, seminars, or other meetings sponsored or cosponsored by NASA.

- SPECIAL PUBLICATION. Scientific, technical, or historical information from NASA programs, projects, and missions, often concerned with subjects having substantial public interest.

- TECHNICAL TRANSLATION. English-language translations of foreign scientific and technical material pertinent to NASA's mission.

Specialized services also include creating custom thesauri, building customized databases, organizing and publishing research results.

For more information about the NASA STI program, see the following:

- Access the NASA STI program home page at *http://www.sti.nasa.gov*

- E-mail your question via the Internet to *help@ sti.nasa.gov*

- Fax your question to the NASA STI Help Desk at 443–757–5803

- Telephone the NASA STI Help Desk at 443–757–5802

- Write to:
  NASA Center for AeroSpace Information (CASI)
  7115 Standard Drive
  Hanover, MD 21076–1320

Investigation of the Mechanical Performance of Compliant Thermal Barriers

Jeffrey J. DeMange
The University of Toledo, Toledo, Ohio

Robert J. Bott
Case Western Reserve University, Cleveland, Ohio

Patrick H. Dunlap
Glenn Research Center, Cleveland, Ohio

National Aeronautics and
Space Administration

Glenn Research Center
Cleveland, Ohio 44135

December 2011

Acknowledgments

Level of Review: This material has been technically reviewed by technical management.

Available from

NASA Center for Aerospace Information	National Technical Information Service
7115 Standard Drive	5301 Shawnee Road
Hanover, MD 21076–1320	Alexandria, VA 22312

Available electronically at http://www.sti.nasa.gov

Investigation of the Mechanical Performance of Compliant Thermal Barriers

Jeffrey J. DeMange
The University of Toledo
Toledo, Ohio 43606

Robert J. Bott
Case Western Reserve University
Cleveland, Ohio 44106

Patrick H. Dunlap
National Aeronautics and Space Administration
Glenn Research Center
Cleveland, Ohio 44135

Abstract

Compliant thermal barriers play a pivotal role in the thermal protection systems of advanced aerospace vehicles. Both the thermal properties and mechanical performance of these barriers are critical in determining their successful implementation. Due to the custom nature of many thermal barriers, designers of advanced spacecraft have little guidance as to the design, selection, and implementation of these elements. As part of an effort to develop a more fundamental understanding of the interrelationship between thermal barrier design and performance, mechanical testing of thermal barriers was conducted. Two different types of thermal barriers with several core insulation density levels ranging from 62 to 141 kg/m^3 were investigated. Room-temperature compression tests were conducted on samples to determine load performance and assess thermal barrier resiliency. Results showed that the loading behavior of these thermal barriers was similar to other porous, low-density, compliant materials, such as elastomeric foams. Additionally, the insulation density level had a significant non-linear impact on the stiffness and peak loads of the thermal barriers. In contrast, neither the thermal barrier type nor the level of insulation density significantly influenced the room-temperature resiliency of the samples.

Nomenclature

A	footprint area (m^2)
f	generic experimental measurement
F	unit load (N/mm)
l	thermal barrier length (mm)
m	mass of thermal barrier insulation (kg)
P	load (N)
V	volume of thermal barrier core (m^3)
w	thermal barrier width (from contact footprint) (mm)
δ_{n+1}	permanent set, cycle n+1 (mm)
Δ_n	maximum displacement, cycle n (mm)
ρ_{rel}	relative density of the thermal barrier core insulation
ρ^*	density of the thermal barrier core insulation (kg/m^3)
ρ_s	density of the aluminosilicate from which the thermal barrier core insulation is made (kg/m^3)

σ	compressive stress (kPa)
A_s	cross-sectional area of thermal barrier core (m^2)
R_n	resiliency, cycle n (%)
U_f^b	bias error in function or measurement
U_f^p	precision error in function or measurement
U_f^t	total uncertainty in function or measurement
$U_{\rho*}^t$	total uncertainty in density
$U_{x,y,...,z}$	individual uncertainties for the measurements making up a given function

I.   Introduction

COMPLIANT thermal barriers are an integral component of the thermal protection systems (TPS) for nearly all aerospace vehicles. These barriers (Fig. 1), usually made from high-temperature ceramic-based fibrous materials, are typically installed in the interface gaps between various components and substructures. Example locations include areas around access panels and doors, control surfaces, gaps between TPS tiles/panels, perimeters of vents and instrumentation components, and within propulsion systems (Fig. 2). The primary role of the thermal barriers is to help protect the underlying components and structures from excessive heating which may be encountered during high-speed vehicle travel. In addition, the barriers must accommodate structural deflections resulting from thermal, aerodynamic, and/or reaction loads without damaging surrounding materials.

Figure 1.   Examples of compliant thermal barriers: blanket thermal barrier (left) and hybrid thermal barrier (right).
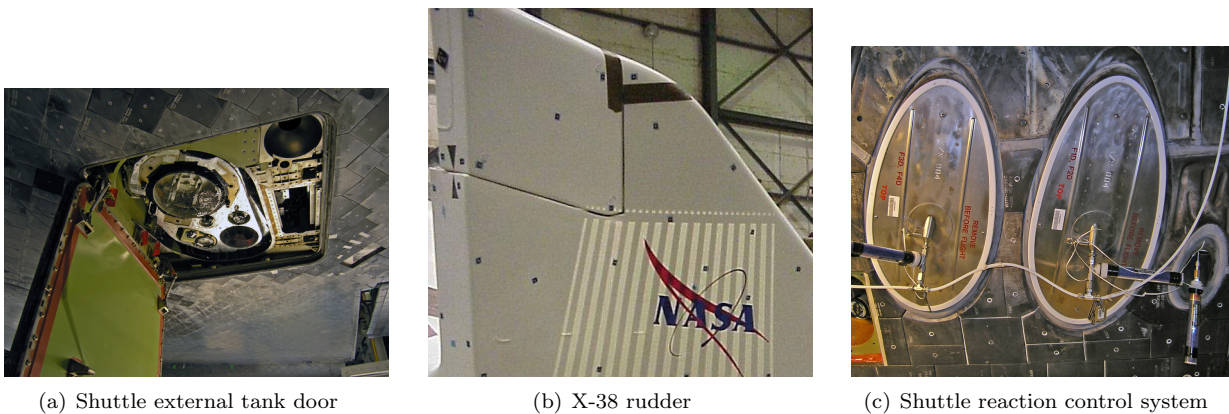

(a) Shuttle external tank door

(b) X-38 rudder

(c) Shuttle reaction control system

Figure 2.   Examples of locations on aerospace vehicles requiring thermal barriers.

Thermal barriers can be fabricated in a multitude of configurations and several parameters can be varied to custom-tailor their performance. Due to the multitude of configurations and often limited performance data, vehicle designers have little guidance on which thermal barrier design to incorporate in a given interface. While it is intuitively obvious the designer needs to assess thermal performance, one must also consider the mechanical behavior of the barriers. With the exception of other application-specific studies conducted by the authors,[1-5] no significant fundamental information on thermal barrier mechanical properties exists in the open literature. An understanding of the load characteristics of the barrier is not only important during a mission, but must also be accounted for in ground operations (e.g., assembly). Excessive loads during any phase of the operations can result in vehicle damage.

In cooperation with the NASA Glenn Research Center, researchers have embarked on an effort to develop a more fundamental understanding of the interrelationship between thermal barrier design and performance. As part of this effort, an investigation was undertaken to evaluate the effect of insulation density on the mechanical properties of thermal barriers. Room-temperature compression tests were performed on two configurations of samples containing several different insulation density levels with load and resiliency results reported herein.

II. Experimental Procedure

A. Test Specimen Description

1. Blanket Thermal Barriers

The blanket thermal barrier (BTB) test specimens were fabricated from two concentric outer sheaths of an aluminoborosilicate woven fabric and a core filled with an aluminosilicate insulation blanket (Fig. 3) at four different density levels: 62, 80, 123, 141 kg/m^3.
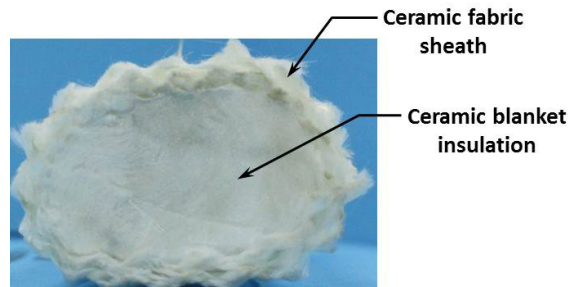

Figure 3. Blanket thermal barrier.

In its as-received form, the aluminosilicate insulation was constructed as a laminated blanket with polycrystalline fibers (mean diameter of 3.0 - 3.5 μm) oriented randomly within the layers (Fig. 4). According to the vendor, the as-received blanket had a nominal density of around 96 kg/m^3. To achieve the desired density levels in the thermal barrier specimens used for the current tests, the blanket was cut to appropriate sizes and then inserted into the sheath layers. The blanket laminate layers were oriented in a slightly curved vertical orientation, as shown in Fig. 3 (i.e., layers predominantly oriented parallel to loading direction). The thermal barriers were also stitched through the thickness using aluminoborosilicate thread. This stitching was implemented as a means to help retain the insulation should the barrier be damaged during an actual flight.

After fabrication was completed, five samples of each density level were cut to length using a dry diamond wheel and then heat-cleaned at 482±11 °C for 15 hrs to remove residual organic sizing. Two to three shorter samples of each density level were also cut and heat-cleaned for density verification. All samples were weighed before and after heat cleaning. The samples were dimensionally measured (width and height) before and after compression testing using a non-contact laser system (Keyence LJ-G200) accurate to within 96 μm. Sample lengths were measured using calipers accurate to 20 μm.
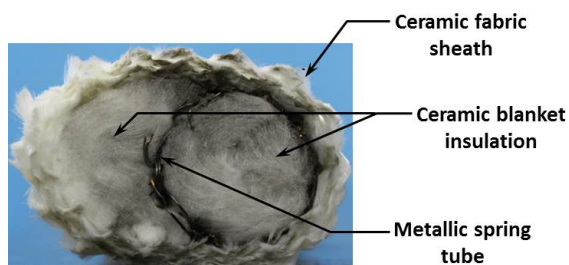
2. Hybrid Thermal Barriers

The hybrid thermal barrier (HTB) test specimens (Fig. 5) were designed to combine the insulating performance of the blanket thermal barrier with the high-temperature resiliency of a metallic spring tube thermal
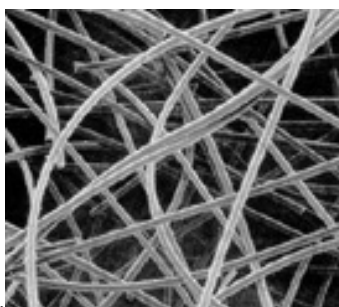
Figure 4. Aluminosilicate fibers in blanket insulation (Courtesy Saffil Ltd.).

barrier. The samples were fabricated by inserting a Rene 41-knitted spring tube (Fig. 6) filled with the aluminosilicate insulation into two outer sheaths of an aluminoborosilicate-woven fabric. The remaining interior volume of the sheath layers was also filled with the insulation. Thermal barrier samples were fabricated using this configuration at two insulation density levels, 76 and 127 kg/m^3. Note that this was the overall average density level for each HTB configuration, inclusive of both the insulation inside and outside of the spring tube. For the insulation outside the spring tube, the layers were generally oriented in a slightly curved vertical configuration (Fig. 5). The insulation inside the spring tubes exhibited more variation between samples in terms of layer orientation.

Figure 5. Hybrid thermal barrier.
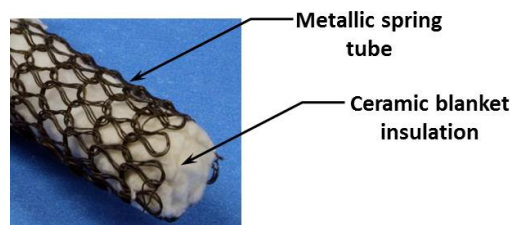
Figure 6. Spring tube (shown with insulation).

Five samples of each density level were cut to length using a dry diamond wheel and heat-cleaned at $482\pm11\,^{\circ}$C for 15 hrs to remove residual organic sizing. Two to three shorter samples of each density level were also cut and heat-cleaned for density verification. All samples were weighed before and after heat cleaning and dimensionally measured (width and height) using a non-contact laser system (Keyence LJ-G200) before and after compression testing. Sample lengths were measured using calipers.

B. Test Facility Description

An MTS Model 318 servohydraulic load frame with custom test fixturing was used to evaluate the load performance of the thermal barrier samples (Fig. 7). The load frame incorporated a 2.2 kN (accurate to within ±0.6 N) load cell to monitor loads during testing. The samples were compressed between two smooth metallic platens. Displacement between the loading platens was measured using a Beta LaserMike Intelliscan 50 laser extensometer (accurate to within approximately $\pm6.4\ \mu$m).

C. Test Procedure

1. Density Estimation

The insulation density of each configuration was determined by sampling several short lengths for each design. After heat-cleaning, weighing, and measuring the dimensions, each density sample was carefully dissected, and all the insulation was removed and weighed. Based upon the laser measurements, a cross-sectional area was estimated assuming an elliptical shape of the thermal barrier core cross section. The corresponding elliptical shapes were then visually compared against the photographs to evaluate the relative accuracy of
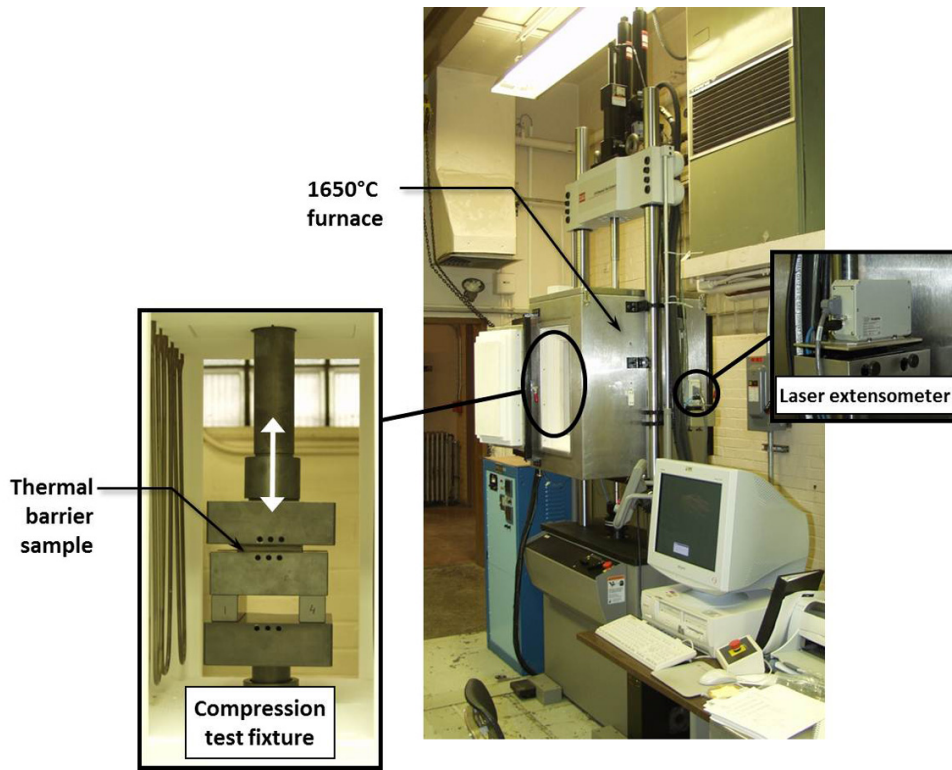
Figure 7. Thermal barrier compression test rig.

the shape assumption. As a confirmation, areas were also measured directly using a commercially available photographic software package. However reference measurements were not always available to accurately scale the areas. In addition, the ends of the thermal barriers often exhibited some local bulging and fraying due to the cutting process and may not have accurately reflected the true cross section of the samples. Additional errors may have been introduced by non-normality of the thermal barrier cross section relative to the camera perspective. Based upon the insulation mass, core area estimate, and the measured length of the sample, the insulation density was calculated according to Eq. (1).

$$\rho^* = \frac{m}{V} = \frac{m}{A_s \cdot l} \tag{1}$$

2. Compression Tests

The thermal barrier samples were compressed at room temperature (approximately $20\,^\circ\text{C}$) between two flat platens to a final gap which corresponded to approximately 30% of their average initial height (i.e., 70% compression). During testing, the samples were loaded to approximately 0.9 N to achieve initial uniform contact and then compressed at a strain rate of roughly 5.0×10^{-3} to the final gap. After dwelling at this gap for approximately 60 s, the samples were unloaded at the same rate to the initial contact point. This load-unload cycle was repeated four times. Prior to the first cycle, a carbon transfer tape was inserted between the top of the sample and the upper platen to generate a contact footprint for compressive stress calculations. After the first cycle, the tape was removed and the setup was adjusted to account for the thickness of the tape. Five samples were tested for each thermal barrier type and density level.

One of the primary responses from the compression tests was load behavior, calculated both in terms of unit loads and stresses. The unit loads were calculated based upon the load and initial length of the specimen (Eq. (2)). The compressive stresses were determined from the loads and contact footprint areas, as per Eq. (3).

$$F = \frac{P}{l} \tag{2}$$

$$\sigma = \frac{P}{A} = \frac{P}{l \cdot w} \tag{3}$$

Thermal barrier resiliency, which is a measure of how well the barrier springs back to its original unde-formed size, was determined after each load cycle using Eq. (4).

$$R_n = \frac{\Delta_n - \delta_{n+1}}{\Delta_n} * 100 \tag{4}$$

A schematic further illustrating the calculation of resiliency is shown in Fig. 8. As shown in this schematic, the resiliency is the amount of compression recovered after unloading from a full cycle of compression. The "per-manent set" in the sample on subsequent cycles is defined as the stroke at which the sample reaches the pre-defined preload value. While resiliency at high temperature is often of prime interest, ambient-temperature resiliency can also be important in terms of ground operations and repeated assembly/disassembly cycles.

(a) Illustration of terms for determining resiliency   (b) Determination of permanent set
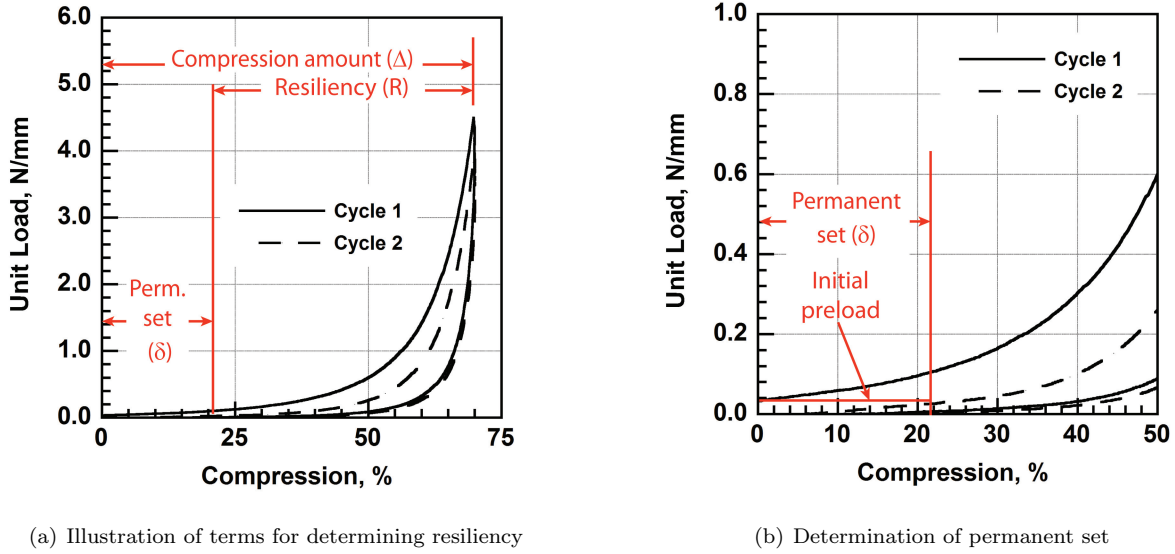
Figure 8. Example plots illustrating calculation of resiliency.

3. Uncertainty Estimation

An uncertainty analysis is an important aspect of any experimental value. The total uncertainties for each measure or calculation (f) were estimated by combining the precision (random) error and the bias (systematic) error, according to Eq. (6).

$$f = f(x, y, \ldots, z) \tag{5}$$

$$U_f^t = \sqrt{(U_f^p)^2 + (U_f^b)^2} \tag{6}$$

For these analyses, the bias and precision error were assumed to be independent.

The precision error for each measure or calculation was determined based upon the standard deviation of the tested samples weighted at a 90% confidence interval. The bias error was estimated by using Eq. (7).

$$U_f^b = \sqrt{\left(\frac{\partial f}{\partial x} U_x\right)^2 + \left(\frac{\partial f}{\partial y} U_y\right)^2 + \ldots + \left(\frac{\partial f}{\partial z} U_z\right)^2} \tag{7}$$

Note that $U_{x,y,\ldots,z}$ are the individual uncertainties for the measurements making up a given function (typically taken as the accuracy of the instrument or estimated based upon prior experience).

# III. Results and Discussion

A.   Density Estimation

Density results from sampling of the thermal barriers are presented in Tables 1 and 2 for the blanket thermal barriers and hybrid thermal barriers, respectively. While a range of density values was obtained, the estimated uncertainties illustrate the potential for some overlap between levels. The uncertainty estimations $(U_{\rho^*}^t)$ are likely somewhat conservative, but also follow from a high sample variability in some cases combined with a limited sample size. This was especially true for the blanket thermal barrier with a core density of 123 kg/m³ and the hybrid thermal barrier at a density level of 127 kg/m³. The uncertainties were also fairly high in general due to the difficulty in obtaining accurate volumetric measurements. This is illustrated in Fig. 9, which shows representative photographs of the ends of the thermal barriers with superimposed ellipse data, as determined from the laser measurements. In some cases, the ellipse assumption appeared to accurately recreate the thermal barrier cross-sectional shape (Fig. 9(a)), while in others, the assumption appeared to overestimate the area (Fig. 9(b)), and thus underestimate the density. Consequently, the high estimated uncertainties are warranted in most cases and indeed seem to be consistent with previous anecdotal experience.

Table 1. Average estimated insulation density results for blanket thermal barriers.

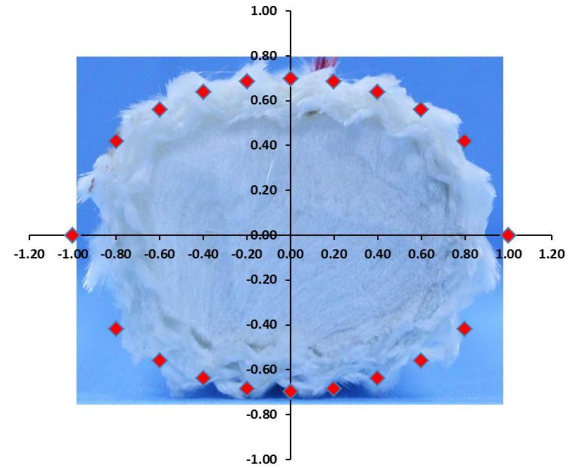| ρ^* $\frac{kg}{m^3}$	$U_{\rho^*}^t$ $\frac{kg}{m^3}$	ρ_{rel}
62	16	0.016
80	26	0.021
123	62	0.031
141	34	0.036

Table 2. Average estimated insulation density results for hybrid thermal barriers.

ρ^* $\frac{kg}{m^3}$	$U_{\rho^*}^t$ $\frac{kg}{m^3}$	ρ_{rel}
76	13	0.019
127	54	0.032
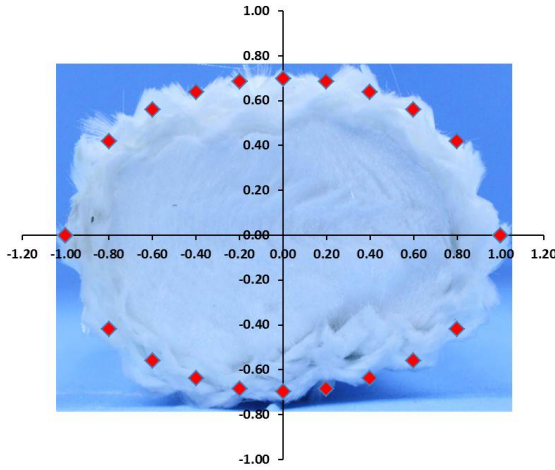
(a) Acceptable fit

(b) Imperfect fit

Figure 9. Examples of conformance of assumed ellipse shape for thermal barrier volume determination (Note: dimensions shown are normalized dimensions).

The tables also include a relative density for the core insulation, which is defined according to Eq. (8)

$$\rho_{rel} = \frac{\rho^*}{\rho_s} \qquad (8)$$

This measure is a fundamental property often used to help characterize the behavior of low-density materials,

such as honeycombs, foams, fiber-based materials, etc. [6] The relative densities presented in the tables are similar to the values typically observed for low-density polymeric foams used for cushioning, packaging, and insulation. [6]

B.   Blanket Thermal Barrier Compression Results

Results from the compression tests for the blanket thermal barriers are presented in Fig. 10 through 12. Note the error bars in each graph denote total uncertainties at 90% confidence intervals. Figures 10(a) and 10(b) show plots of peak unit load and peak compression stress at 70% compression, respectively, as functions of compression cycle for the four insulation density levels. These graphs can aid the designer in conducting structural analyses and determining what insulation density level should be used for thermal barriers placed against specific TPS materials, given material strengths.

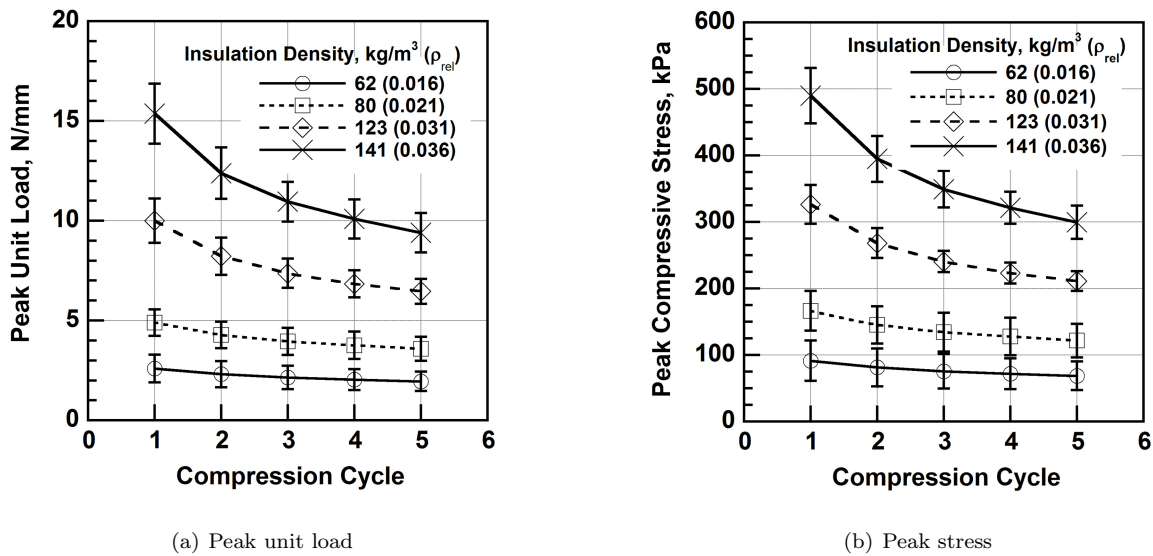
(a) Peak unit load

(b) Peak stress

Figure 10. Blanket thermal barrier peak loads vs. compression cycle.

As shown in both plots, the peak loads increased significantly with increasing core density. For example, peak loads for the first compression cycle escalated by a factor of 6X when the core density increased from 62 to 141 kg/m^3 (i.e., 2.3X increase). This trend is more clearly illustrated in Fig. 11, which shows peak loads as a function of core density for compression cycles 1 and 5. As illustrated in the graph, the loads appeared to increase in a non-linear fashion, especially as the insulation density approached the highest level (141 kg/m^3). With increasing insulation density, core porosity decreased and therefore resulted in more fiber-to-fiber contact (and subsequently higher loads) as the sample was compressed. This type of behavior is also typically observed for low-density elastomeric foams. [6]

Figures 10(a) and 10(b) also show that peak loads decreased with each subsequent compression cycle. This was likely the result of some compaction or "set" in the thermal barriers, possibly due to fiber entanglement, inter-fiber friction, or fiber breakage as the samples were repeatedly compressed. For the blanket thermal barriers, this effect appeared to be more acute at higher core densities. For example, the peak load decreased by approximately 39% after five load cycles for samples with an average core density of 141 kg/m^3. In contrast, peak loads diminished by approximately 25% for samples with an average insulation density of 62 kg/m^3.

Plots showing load behavior as a function of percent compression during the first load cycle for the different insulation density levels are presented in Figures 12(a) and 12(b). As shown in Fig. 12(b), both the load and displacement were normalized to produce what essentially amounts to a stress-strain curve. Due to the porous nature of the thermal barriers and the somewhat compliant behavior of the fiber-based blanket, the compressive response of these barriers was similar to that exhibited by low-density foam materials, such as polyethylene. [7-9] For open-celled polymeric foams, the stress-strain curves exhibit shapes similar to that shown in Fig. 13. This response is composed of a small region of linear elasticity, followed by a plateau
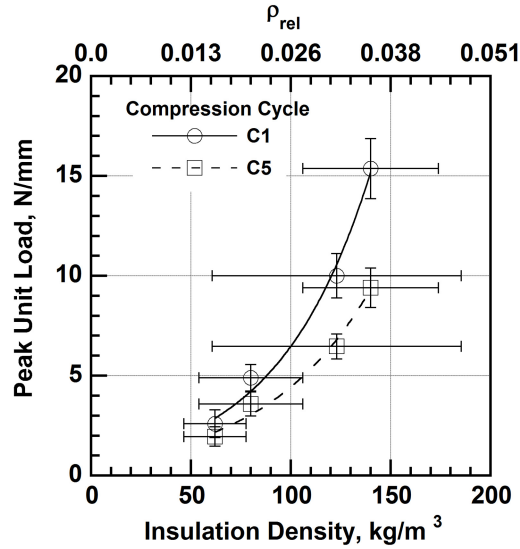
Figure 11. Blanket thermal barrier peak unit load vs. core insulation density.

regime, and finally a densification region. The deformation mechanics for these foams have been shown to involve cell wall bending (linear-elastic region), followed by wall buckling (plateau region), and then finally cell collapse and densification.[6]
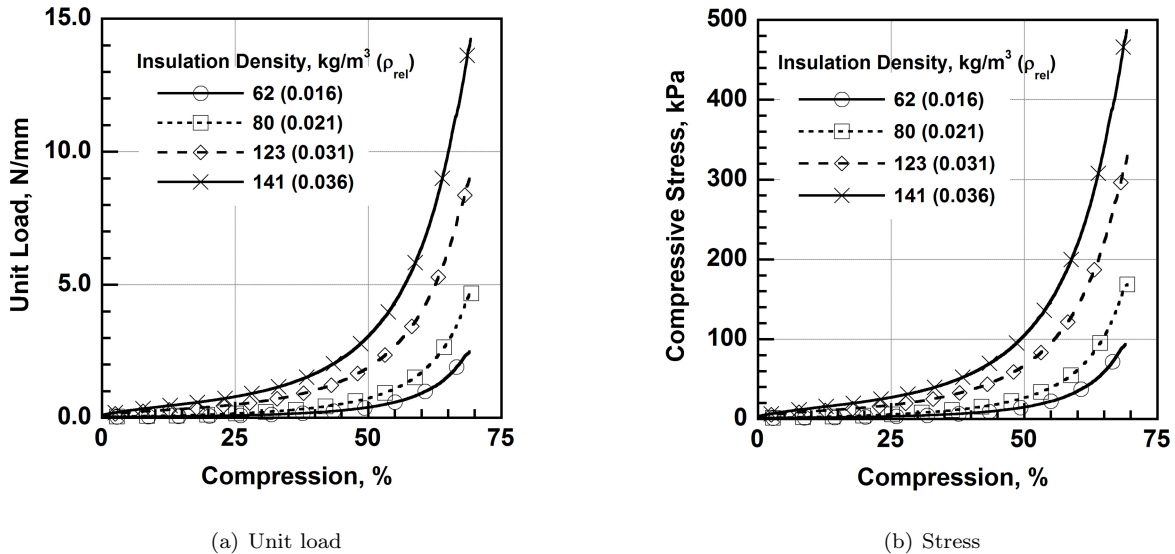

(a) Unit load

(b) Stress

Figure 12. Blanket thermal barrier load vs. percent compression.

This same behavior is evident in Fig. 12(b) for the thermal barriers, though the influence of the insulation blanket layers plays an additional role at a macro-level. In addition, there is not a clear differentiation between the linear-elastic region and the plateau region in many cases. A closer examination of the deformation mechanics of the thermal barrier (Fig. 14) illustrated that as the barrier was compressed, the blanket layers further bent over. With continued deformation, the layers rotated to an orientation in which the through-thickness direction was nearly parallel to the loading direction. Similar to conventional foams, the porosity in the samples increasingly collapsed and more fiber-to-fiber contact occurred as the specimens were further compressed. Correspondingly, the stiffness increased with additional compression as the insulation material
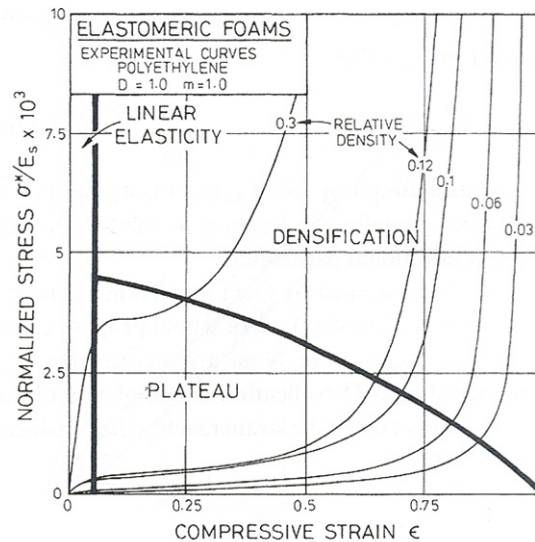
Figure 13. Compression performance of polyethylene as a function of relative density. [6]

densified. As observed with other low-density porous materials, the stiffness increased more rapidly for samples with higher core densities (and therefore lower initial porosity).

It should be noted that it was only possible to determine the contact area at maximum compression (i.e., the carbon transfer tape only captured a final footprint). Therefore the compression stresses at lower compression levels were slightly underestimated. Nevertheless, the impact of insulation density on load behavior is clearly evident in Fig. 12(b). Additionally this data can guide maximum acceptable thermal barrier compression levels given the mating material compressive strength.

Blanket thermal barrier resiliency results (after being compressed by 70% during each load cycle) are presented in Fig. 15. As illustrated in this plot, the blanket thermal barriers exhibited approximately 20-30% permanent set after the first load cycle at ambient temperatures. The samples continued to compact with additional load cycling. This behavior would need to be considered if multiple assembly/disassembly cycles which repeatedly compress the thermal barriers to high levels would occur during ground operations. Although the plots appear to suggest improved resiliency with increased core density, this effect is not statistically significant when the uncertainty in the data is considered. Therefore thermal barrier resiliency likely cannot be improved by increasing insulation density.

C. Hybrid Thermal Barrier Compression Results

Compression results for the hybrid thermal barrier samples are presented in Figures 16 and 17. In general, these samples exhibited load behavior similar to that of the blanket thermal barriers. A higher insulation core density resulted in higher peak loads. As an example, the peak loads for the first compression cycle were approximately 2.5X higher when the core density increased from 76 to 127 kg/m^3. By comparison, the peak loads for the blanket thermal barriers increased by a factor of 2.0X across the same approximate density change.

As with the blanket thermal barriers, the peak loads decreased with increasing cycling (Fig. 16). It was initially assumed that the hybrid thermal barrier, with its integral spring tube, would exhibit better resiliency and maintain peak loads better than the blanket thermal barriers. Surprisingly, the average load decrease after five compression cycles for HTB samples with an average density of 76 kg/m^3 was 36%. As shown in Table 3, this was a greater load drop than that observed with the blanket thermal barriers (27% load decrease) at a similar density level.

As indicated previously, Figure 16 illustrates that at similar density levels, the hybrid thermal barriers generally exhibited higher peak loads than the blanket thermal barriers. This was most evident for the higher density samples (120 - 130 kg/m^3). The additional stiffening of these types of thermal barriers was

(a) Initial (undeformed)

(b) 10% Compression

(c) 30% Compression

(d) 70% Compression

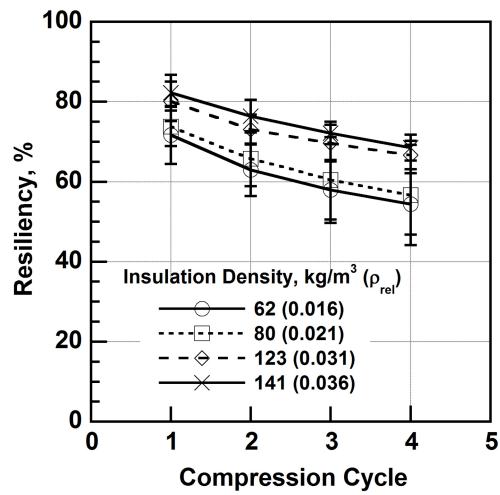**Figure 14. Representative blanket thermal barrier at various compression levels.**

Figure 15. Blanket thermal barrier resiliency vs. compression cycle.
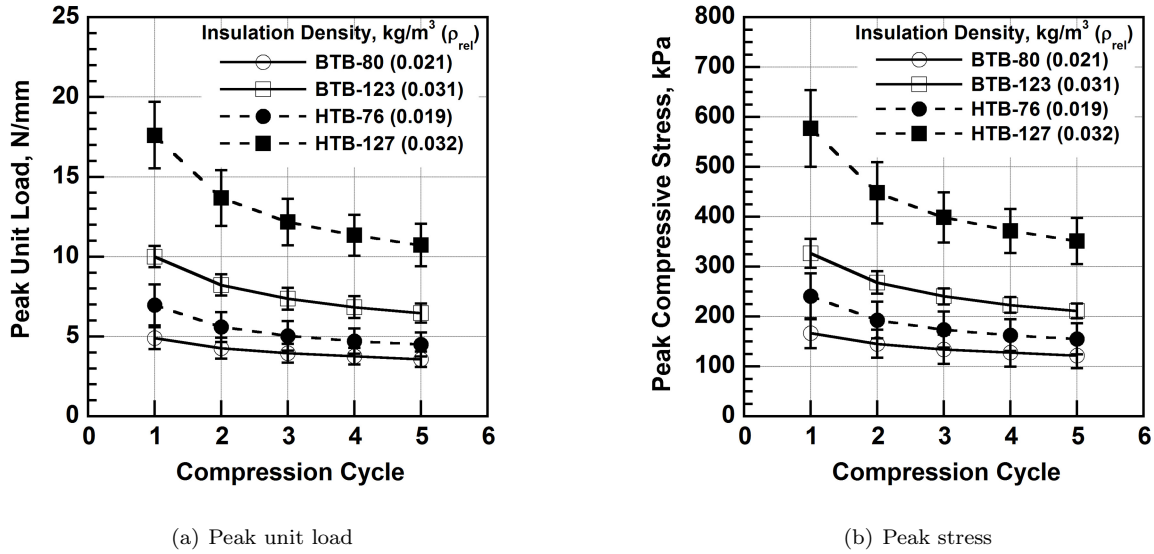
(a) Peak unit load   (b) Peak stress

Figure 16. Blanket thermal barrier (BTB) and hybrid thermal barrier (HTB) peak loads vs. compression cycle.

Table 3. Average decrease in load after five cycles for blanket thermal barriers and hybrid thermal barriers.

ρ^*	Unit Load, N/mm		Decrease
$\frac{kg}{m^3}$	Cycle 1	Cycle 5	%
Blanket Thermal Barriers			
62	2.6	2.0	23
80	4.9	3.6	27
123	10.0	6.5	35
141	15.4	9.4	39
Hybrid Thermal Barriers			
76	7.0	4.5	36
127	17.6	10.7	39

likely a result of the spring tube stiffness[4] as well as the additional constraint imposed by the spring tube on the insulation as the barriers were deformed. This would seem to coincide with the effect becoming more acute at higher density levels.

Plots of unit load and compressive stress as functions of percent compression are presented in Figures 17(a) and 17(b), respectively. These graphs compare the effect of similar density levels for the blanket thermal barriers and hybrid thermal barriers. In general, the loading behavior of the hybrid thermal barriers was similar to the blanket thermal barriers, indicating similar deformation mechanisms were occuring. The augmented stiffness of the hybrid thermal barriers when compared to the blanket thermal barriers is further illustrated in these plots.

Figure 18 compares the room-temperature resiliency between the two types of thermal barriers. As illustrated, no significant improvement in resiliency was observed for the hybrid thermal barrier at room temperature, even though they incorporated a resilient spring tube element. The reasons for this behavior are unclear, but may be related to an insufficient restoring force in the spring tube when the surrounding
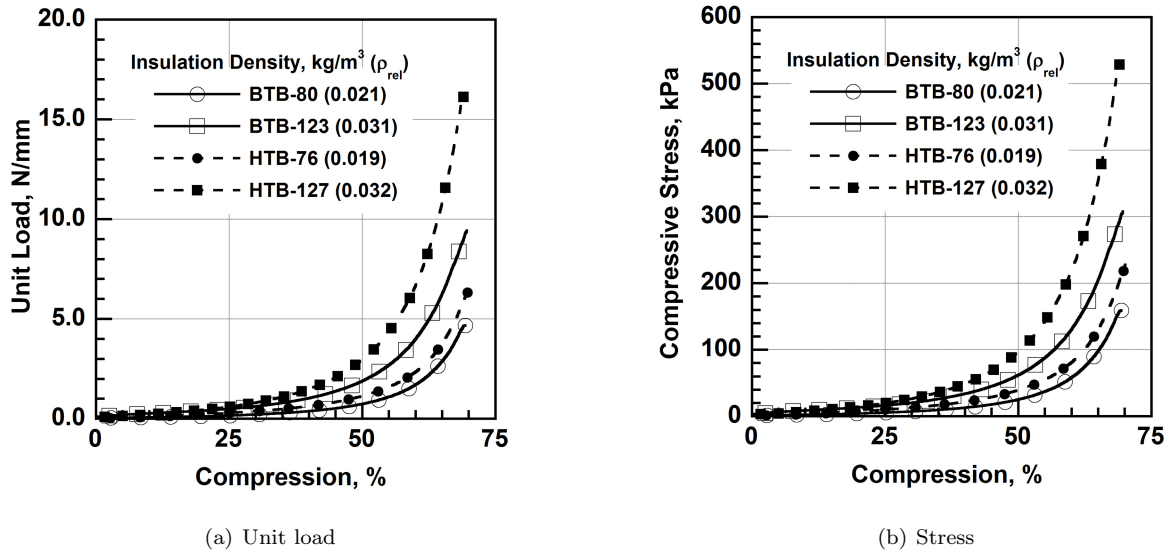
(a) Unit load   (b) Stress

Figure 17. Blanket thermal barrier (BTB) and hybrid thermal barrier (HTB) loads vs. percent compression.

volumes are filled with insulation. Therefore the resiliency in the thermal barrier appeared to be dominated at room temperature by the performance of the insulation. The high-temperature resiliency would be expected to demonstrate a performance advantage for the hybrid thermal barrier. Though no significant improvement in resiliency was observed, recent testing of these barriers in high-temperature arc jet testing simulating reentry has indicated some thermal advantage of the hybrid version.[10]
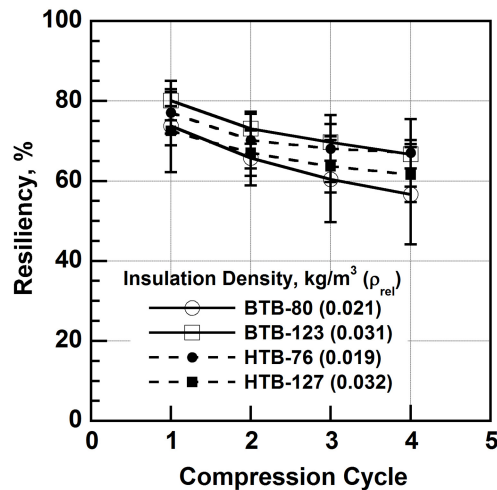
Figure 18. Blanket thermal barrier (BTB) and hybrid thermal barrier (HTB) resiliency vs. compression cycle.

IV. Conclusions

Compliant thermal barriers are an integral part of the thermal protection systems of nearly all advanced aerospace vehicles. However, designers of modern aerospace vehicles often have little guidance on the proper design, selection, and implementation of thermal barriers. To that end, a study was initiated to begin to gain a more fundamental understanding of thermal barrier configuration versus performance. Room-temperature

compression tests up to approximately 70% compression were conducted on two types of thermal barriers: (a) a blanket thermal barrier which contained only aluminosilicate insulation in the core and (b) a hybrid thermal barrier which also included a metallic-knitted spring tube as part of the core, in addition to the insulation. For each thermal barrier type, several different levels of core insulation density were evaluated, ranging from 62 to 141 kg/m^3.

Results showed that in general, the load behavior of the thermal barriers was very similar to that of other complaint low-density materials, such as elastomeric foams. The load profiles were essentially linear up to approximately 20-30% compression and then exhibited significant non-linear increases in loads as the samples were compressed and the core porosity decreased. The level of core density had a significant non-linear effect on barrier stiffness and peak loads. As an example, an increase of insulation density by 2.3X resulted in a peak load increase of approximately 6X for the blanket thermal barrier type. In contrast, the thermal barriers exhibited little sensitivity to type or core insulation density on barrier resiliency at ambient temperature. These results provide a basis for proper thermal barrier design, selection, and implementation and offer the potential for future modeling efforts.

References

[1] Dunlap, P. H., Steinetz, B. M., and Curry, D. M., "Rudder/fin seal investigations for the X-38 re-entry vehicle," *Proceedings of the 36th AIAA/ASME/SAE/ASEE Joint Propulsion Conference & Exhibit*, No. AIAA-2000-3508, AIAA, Huntsville, AL, 16-19 July 2000.

[2] Dunlap, P. H., Steinetz, B. M., Curry, D. M., Newquist, C. W., and Verzemnieks, J., "Further investigations of control surface seals for the X-38 re-entry vehicle," *Proceedings of the 37th AIAA/ASME/SAE/ASEE Joint Propulsion Conference & Exhibit*, No. AIAA-2001-3628, AIAA, Salt Lake City, UT, 8-11 July 2001.

[3] Dunlap, P. H., Steinetz, B. M., Curry, D. M., DeMange, J. J., Rivers, H. K., and Hsu, S.-Y., "Investigations of Control Surface Seals for Re-Entry Vehicles," *Proceedings of the 38th AIAA/ASME/SAE/ASEE Joint Propulsion Conference & Exhibit*, No. AIAA-2002-3941, AIAA, Indianapolis, IN, 7-10 July 2002.

[4] Taylor, S. C., DeMange, J. J., Dunlap, P. H., and Steinetz, B. M., "Evaluation of High Temperature Knitted Spring Tubes for Structural Seal Applicationse," *Proceedings of the 40th AIAA/ASME/SAE/ASEE Joint Propulsion Conference & Exhibit*, No. AIAA-2004-3890, AIAA, Fort Lauderdale, FL, 11-14 July 2004.

[5] DeMange, J. J., Dunlap, P. H., and Steinetz, B. M., "Improved Seals for High Temperature Airframe Applications," *Proceedings of the 42nd AIAA/ASME/SAE/ASEE Joint Propulsion Conference & Exhibit*, No. AIAA-2006-4935, AIAA, Sacramento, CA, 9-12 July 2006.

[6] Gibson, L. J. and Ashby, M. F., *Cellular Solids - Structures and Properties, 2nd Ed.*, Cambridge University Press, Cambridge, UK, 1997.

[7] Yang, L. M. and Shim, V. P. W., "A visco-hyperelastic constitutive description of elastomeric foam," *International Journal of Impact Engineering*, Vol. 30, 2004, pp. 1099–1110.

[8] Wang, B., Peng, A., Zhang, Y., and Zhang, Y., "Compressive response and energy absorption of foam EPDM," *Journal of Applied Polymer Science*, Vol. 105, 2007, pp. 3462–3469.

[9] Zhang, J., Kikuchi, N., Li, V., Yee, A., and Nusholtz, G., "Constitutive modeling of polymeric foam material subject to dynamic crash loading," *International Journal of Impact Engineering*, Vol. 21, No. 5, 1998, pp. 369–386.

[10] Finkbeiner, J., Mayer, J., Creager, C., Delgado, I., DeMange, J., Dunlap, P., and Steinetz, B., "Report for the Orion Back Shell Interface Thermal Protection System Arc Jet Tests," Tech. Rep. OTPS-0023, 7 February 2011.

1. REPORT DATE (DD-MM-YYYY) 01-12-2011	2. REPORT TYPE Technical Memorandum	3. DATES COVERED (From - To)

4. TITLE AND SUBTITLE Investigation of the Mechanical Performance of Compliant Thermal Barriers	5a. CONTRACT NUMBER NNC08CA35C
	5b. GRANT NUMBER
	5c. PROGRAM ELEMENT NUMBER
6. AUTHOR(S) DeMange, Jeffrey, J.; Bott, Robert, J.; Dunlap, Patrick, H.	5d. PROJECT NUMBER
	5e. TASK NUMBER
	5f. WORK UNIT NUMBER WBS 644423.06.31.03.08.03

7. PERFORMING ORGANIZATION NAME(S) AND ADDRESS(ES) National Aeronautics and Space Administration John H. Glenn Research Center at Lewis Field Cleveland, Ohio 44135-3191	8. PERFORMING ORGANIZATION REPORT NUMBER E-17879

9. SPONSORING/MONITORING AGENCY NAME(S) AND ADDRESS(ES) National Aeronautics and Space Administration Washington, DC 20546-0001	10. SPONSORING/MONITOR'S ACRONYM(S) NASA
	11. SPONSORING/MONITORING REPORT NUMBER NASA/TM-2011-217142

12. DISTRIBUTION/AVAILABILITY STATEMENT
Unclassified-Unlimited
Subject Categories: 18, 27, and 39
Available electronically at http://www.sti.nasa.gov
This publication is available from the NASA Center for AeroSpace Information, 443-757-5802

13. SUPPLEMENTARY NOTES

14. ABSTRACT
Compliant thermal barriers play a pivotal role in the thermal protection systems of advanced aerospace vehicles. Both the thermal properties and mechanical performance of these barriers are critical in determining their successful implementation. Due to the cus- tom nature of many thermal barriers, designers of advanced spacecraft have little guidance as to the design, selection, and implementation of these elements. As part of an effort to develop a more fundamental understanding of the interrelationship between thermal bar- rier design and performance, mechanical testing of thermal barriers was conducted. Two different types of thermal barriers with several core insulation density levels ranging from 62 to 141 kg/m^3 were investigated. Room-temperature compression tests were conducted on samples to determine load performance and assess thermal barrier resiliency. Results showed that the loading behavior of these thermal barriers was similar to other porous, low-density, compliant materials, such as elastomeric foams. Additionally, the insulation density level had a significant non-linear impact on the stiffness and peak loads of the thermal barriers. In contrast, neither the thermal barrier type nor the level of insulation density significantly influenced the room-temperature resiliency of the samples.

15. SUBJECT TERMS
Seals; Thermal insulation; Thermal barriers; Thermal protection; Load test; Compression loads; Mechanical properties

16. SECURITY CLASSIFICATION OF:			17. LIMITATION OF ABSTRACT	18. NUMBER OF PAGES	19a. NAME OF RESPONSIBLE PERSON STI Help Desk (email:help@sti.nasa.gov)
a. REPORT U	b. ABSTRACT U	c. THIS PAGE U	UU	20	19b. TELEPHONE NUMBER (include area code) 443-757-5802